Exchange gate in solid-state spin-quantum computation: The applicability of the Heisenberg model

V. W. Scarola and S. Das Sarma
Condensed Matter Theory Center, Department of Physics, University of Maryland, College Park, Maryland 20742-4111, USA
(Received 20 October 2004; published 24 March 2005)

Solid-state quantum-computing proposals rely on adiabatic operations of the exchange gate among localized spins in nanostructures. We study corrections to the Heisenberg interaction between lateral semiconductor quantum dots in an external magnetic field. Using exact diagonalization we obtain the regime of validity of the adiabatic approximation. We also find qualitative corrections to the Heisenberg model at high magnetic fields and in looped arrays of spins. Looped geometries of localized spins generate flux-dependent multispin terms which go beyond the basic Heisenberg model.

DOI: 10.1103/PhysRevA.71.032340 PACS number(s): 03.67.Pp, 03.67.Lx

I. INTRODUCTION

Scalable quantum-computation proposals, particularly in solid-state architectures compatible with existing microelectronic technology, are of great potential importance. The exchange gate [1], based on the Heisenberg interaction between localized spins, is a key concept underlying several proposed quantum- computer architectures in semiconductor nanostructures, where the spin of a localized electron serves as the single qubit. [1–4]. In most spin-based quantum-computer proposals single-qubit operations involve rotations of individual spins by external magnetic field pulses (essentially a modified electron spin resonance technique implemented on individual spins) or by some other techniques (e.g., local *g*-factor manipulation by external electric field pulses). The two-qubit operation in solid-state spin architectures is projected to be achieved by the exchange-gate operation. The ability of a tunable exchange gate (which enables the exchange coupling to change from zero to a finite value within a "reasonable" gating time) in carrying out the SWAP operation leads to the implementation of the universal two-qubit Controlled-NOT gate which, along with single-qubit gates, provides a universal set of quantum gates. The perceived advantages of solid-state quantum computation are its scalability (because of the existing semiconductor microelectronics infrastructure), the low decoherence rate for spin states (as compared, for example, with charge states in semiconductors), and the feasibility of precise control over the local interelectron Heisenberg coupling through the exchange gate. Among the disadvantages is the inevitable presence of some spin decoherence due to the background solid-state environment [5] and difficulties in the measurement of single-electron-spin states. However, recent experimental advances [6] have demonstrated single-spin measurements of localized electrons embedded in semiconductors.

In this work we provide a detailed and quantitatively accurate theoretical study of two complementary aspects of solid-state spin-quantum-computer architectures. First, we develop a theory for obtaining an accurate map of the low-lying Hilbert space of the quantum-dot-based spin-quantum-computer architecture (the Loss-DiVincenzo [1] architecture in coupled GaAs quantum dots) in the presence of an external magnetic field. Our calculation of the Hilbert space structure of the coupled quantum dot (with one electron on each dot) system differs from earlier work on the problem in the sense that it is essentially exact for our model. [7,8]. Earlier work obtaining the Hilbert space structure of the coupled double-dot quantum computer system used perturbative approximations akin to Heitler-London or Hund-Mulliken theories [9,10]. As explained later in this paper we manage to carry out an exact numerical diagonalization of the two-electron coupled-dot interaction Hamiltonian by borrowing theoretical techniques that have been extremely successful in elucidating the ground-and excited-state properties of the strongly correlated fractional quantum Hall system. Second, we describe and discuss (again using the exact diagonalization technique as the theoretical tool) a subtle topological feature of a certain class of solid-state spin ("cluster") qubits, which have attracted considerable recent attention, where clusters of spins are cleverly aligned to serve as qubits (rather than just single spins) offering certain advantages in quantum computation [11–14]. We show that in looped geometries these spin-cluster qubits have higher-order spin interaction terms (three-spin, four-spin, etc., terms) arising from chiral interaction terms which will have serious adverse consequences for quantum computation by providing nontrivial flux dependence which must be taken into account [15]. Our finding of the chiral Hamiltonian in spin-cluster qubits may have possible consequences for all spin-quantum-computing architectures (and not just the semiconductor-nanostructure-based ones [16]). Again, the exact diagonalization technique is the theoretical method we employ to demonstrate, validate, and quantify the chiral spin Hamiltonian.

The common theme running through the two complementary topics studied in this work is a thorough investigation of the precise applicability of the Heisenberg Hamiltonian as a description of the spin interaction in exchange-gate quantum-computer architectures. In particular, we are interested in figuring out the limitations and the constraints on the Heisenberg interaction model as the underlying Hamiltonian for exchange-gate, two-qubit entanglement in the presence of an external magnetic field. In this context we also want to know what, if any (and how large), the correction terms are to the

Heisenberg model description of the exchange-gate quantum dynamics in the solid-state spin-based quantum computer. This study is motivated by the fact that precise knowledge of the exact Hamiltonian controlling the qubit dynamics is absolutely essential in developing quantum-computing algorithms (and architectures) since in quantum computation the Hamiltonian itself determines the programming codes. We must, therefore, know the Hamiltonian precisely.

To study modifications to the Heisenberg Hamiltonian in tunnel-coupled single-electron quantum dots in an external magnetic field we consider a realistic Hamiltonian involving an equal number of parabolic quantum dots and electrons interacting through the Coulomb interaction. We find deviations from simple Heisenberg behavior where expected, when the quantum dots are strongly coupled and under intense magnetic fields. We find, using a variational ansatz [17] and exact diagonalization, that at high magnetic fields the two-electron orbital states may be characterized by a vorticity. We define vorticity as the number of zeros attached to each electron in the many-body wave function through the term $(z_i - z_j)^p$, where $z = x + iy$ is a complex coordinate in the x-y plane and the integer p is the vorticity of the state. We find level repulsion between states with either even or odd vorticity. We identify the parameter regime required to maximize level repulsion among wanted and unwanted states, ensuring adiabatic operation of the exchange gate.

Using perturbation theory applied to the extended Hubbard model we find other qualitative modifications to the Heisenberg interaction among weakly tunnel-coupled quantum dots. We find that in spin clusters formed from loops of three or more spins, many-spin terms couple to external sources of flux. We focus, numerically, on the triangular configuration in particular. Here, we show quantitatively that a three-spin chiral term couples to flux through the triangle. [15]. We investigate both the low- and high-magnetic-field regimes and model the effective spin Hamiltonian in terms of two parameters: the flux passing through the triangle *and* the vorticity (or effective flux) attached to each electron. We go on to study four-spin configurations where three- and four-body terms modify the Heisenberg interaction. [10]. We find that four- body terms depend on the flux through closed loops as well.

Implementations of exchange-based-only quantum computation with the least overhead, from a quantum-computing perspective, involve several spins interacting simultaneously through the Heisenberg interaction, although this is not necessary. One may consider algorithms involving no more than two simultaneously coupled spins or geometries which exclude closed loops of spins. In what follows we analyze a special case: looped geometries of simultaneously interacting single-spin quantum dots which, as we will show, necessarily involve flux dependence.

In Sec. II we present a model of several lateral, single-electron quantum dots in an external magnetic field. The model establishes four regimes defined by parameters related to confinement, the external magnetic field, and interdot separation. In Sec. II A we relate the coupled-quantum-dot model to a fourth-order spin Hamiltonian based on well-known perturbation theories of the extended Hubbard model. Here, we broaden this treatment to include magnetic field effects. We find many-body spin terms which couple to external magnetic fields. In Sec. II B we describe a variational theory of the many-dot problem which accesses nonperturbative regimes of the parameter space. In Sec. III we discuss implications of the perturbative and variational treatments for qubit proposals involving two, three, and four coupled spins. In Sec. IV A we use exact diagonalization of a physically plausible Coulomb Hamiltonian to explore the low-energy Hilbert space of two coupled single-electron quantum dots. We find that the variational ansatz agrees with exact results. The results suggest that electrons in coupled quantum dots capture vortices of the many-body wave function to screen the Coulomb interaction, at high fields. In Sec. IV B we compare exact diagonalization results of three coupled single-electron quantum dots with the spin Hamiltonian derived using perturbation theory. We show numerically that chiral three-spin terms couple the spin states of a decoherence-free subsystem to external sources of enclosed flux. We parametrize the magnetic field behavior of the lowest spin states with a spin Hamiltonian that depends on the enclosed flux and the number of vortices (or effective flux [17]) attached to each electron. We conclude in Sec. V.

II. MODEL

We study the low-energy Hilbert space of N lateral quantum dots containing N electrons lying in the x-y plane with the following Hamiltonian:

$$H = \sum_{i=1}^{N} \left[\frac{1}{2m^*}\left(\mathbf{p}_i + \frac{e}{c}\mathbf{A}_i\right)^2 + V_N(\mathbf{r}_i) \right] + \sum_{i<j}^{N} \frac{e^2}{\varepsilon|\mathbf{r}_i - \mathbf{r}_j|} + g^* \mu_B \mathbf{S}\cdot\mathbf{B}. \qquad (1)$$

We focus on GaAs. In which case we have an effective mass $m^* = 0.067 m_e$, dielectric constant $\varepsilon = 12.4$, and g factor $g^* = -0.44$. We work in the symmetric gauge with magnetic field $\mathbf{B} = B\hat{z}$. $\mathbf{S}$ is the total spin. The single-particle potential confines the electrons to lie in parabolic wells centered at N positions $\mathbf{R}_i$:

$$V_N(\mathbf{r}) = \frac{m^*\omega_0^2}{2} \min\{|\mathbf{r} - \mathbf{R}_1|^2, \ldots, |\mathbf{r} - \mathbf{R}_N|^2\}, \qquad (2)$$

where ω_0 is a parabolic confinement parameter which may be compared to the cyclotron frequency $\omega_c = eB/m^*c$. The confining potential localizes the electrons at N sites with intersite separation $R = |\mathbf{R}_i - \mathbf{R}_j|$. R may be compared to the modified magnetic length $a = \sqrt{\hbar c/eB}(1 + 4\omega_0^2/\omega_c^2)^{-1/4}$. Solutions of the above Hamiltonian take the form $\mathcal{A}[|\psi\rangle \otimes |\lambda\rangle_N]$ where $|\psi\rangle$ and $|\lambda\rangle_N$ are the orbital and spin parts of the wave function, $\mathcal{A}$ is the antisymmetrization operator, and the subscript denotes the number of electrons and quantum dots.

The parameters in H define several regimes relevant for quantum-computing architectures utilizing similarly confined single-electron quantum dots in an external magnetic field. Figure 1 depicts four separate pieces of the parameter space with the confinement parameter ω_0 fixed. The solid line encloses an area in which the excited, orbital states of the quantum dots have high energy Δ, and the interdot coupling be-

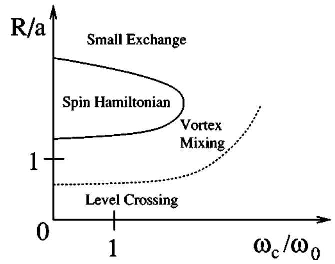

FIG. 1. Schematic showing four regions characterizing spin and orbital degrees of freedom in several coupled quantum dots defined by the parameters in Eq. (1) at fixed confinement ω_0. The vertical axis depends on the interdot spacing R, while the horizontal axis depends on the ratio between the cyclotron frequency ω_c and ω_0. The region of interest for quantum computing (spin Hamiltonian) yields a spin Hamiltonian dominated by Heisenberg exchange coupling $J_{ij}\mathbf{S}_i\cdot\mathbf{S}_j$. Here, the higher orbital energy levels of the quantum dot have much higher energy than the exchange splitting, $\Delta \gg J$. Above this region, $R/a \gg 1$, the electrons in each dot do not interact strongly. At high magnetic fields and near $R/a \sim 1$, the electrons capture vortices of the many-body wave function to form mixtures with $\Delta \gtrsim J$. Below the dotted line the small separation between dots allows single-dot behavior, and therefore level crossing, $\Delta \lesssim J$.

tween two dots maps onto the Heisenberg Hamiltonian $J_{12}\mathbf{S}_1\cdot\mathbf{S}_2$, as originally envisaged in Ref. [1]. We show, using both perturbation theory in the Hubbard limit (Sec. II A) and exact diagonalization (Sec. IV B), that in this regime several coupled quantum dots, $N>2$, involve symmetry-breaking many-spin terms with nontrivial flux field dependence. Above the spin Hamiltonian regime ($R/a \gg 1$) weak interdot tunneling yields a small exchange interaction. Below the dashed line, higher orbital states of the quantum dot have a particularly low energy and therefore mix with the low-energy states of the quantum dot, $\Delta \lesssim J$. This regime is characterized by magnetic-field-dependent level crossings among potential qubit spin states and unwanted higher energy levels of the double-dot system. Between the level crossing and spin Hamiltonian regimes we find, using a combination of exact diagonalization (Sec. IV) and variational techniques (Sec. II B), that electrons in the dots capture vortices of the N-body wave function to screen the strong Coulomb interaction. Here we find that the first excited state of the many-dot system mixes vorticity leaving the unwanted excited states of the quantum dot somewhat higher in energy than the spin splitting between the lowest states, $\Delta \gtrsim J$. In Sec. II we discuss how these regimes pertain to qubit proposals utilizing coupled quantum dots.

A. Perturbative expansion

We first seek an approximation to Eq. (1) that qualitatively captures the structure of the low-energy Hilbert space in terms of on-site spin operators in the limit of weak intersite coupling. Such a Hamiltonian may be used to define qubit gates among spins localized in neighboring quantum dots. We work in the single-band, tight-binding limit, a good approximation in the limit $\Delta \gg J$. We also take the on-site Coulomb interaction to be much larger than the tunneling energy. As a result we may also restrict our attention to singly occupied states. As a first approximation we then obtain the extended Hubbard Hamiltonian:

$$H_H = -\sum_{i,j,\alpha\in\uparrow\downarrow} t_{ij}c^\dagger_{i\alpha}c_{j\alpha} + U\sum_i n_{i\uparrow}n_{i\downarrow} + V\sum_{i,(\alpha,\alpha')\in\uparrow\downarrow} n_{i,\alpha}n_{i+1,\alpha'} + g^*\mu_B\mathbf{B}\cdot\sum_i \mathbf{S}_i, \quad (3)$$

where $c^\dagger_{i\alpha}$ creates a fermion at the site i with spin α and $n_{i\alpha}=c^\dagger_{i\alpha}c_{i\alpha}$. H_H incorporates the on-site spin operators $\mathbf{S}_i=\frac{1}{2}c^\dagger_{i\alpha}\boldsymbol{\sigma}_{\alpha\alpha'}c_{i\alpha'}$, where $\boldsymbol{\sigma}$ are the Pauli matrices. In the presence of an external magnetic field the tunneling coefficients are complex: $t_{ij}=|t_{ij}|\exp(2\pi i\Phi_{ij}/\Phi_0)$, where $\Phi_0\equiv hc/e$ is the flux quantum. The magnetic vector potential generates the Peierls phase

$$\Phi_{ij} = \int_i^j \mathbf{A}\cdot d\mathbf{r}, \quad (4)$$

where the integral runs along a path connecting the sites i and j. Working in the limit $|t_{ij}|/U \ll 1$ and $v\equiv V/U \ll 1$ we can self-consistently confine our attention to the single-occupancy states of the full Hilbert space. For large v the extended Hubbard term favors double occupancy and our approximation breaks down. We consider this regime variationally in the next section.

We expand H_H by applying a unitary transformation $\exp(iK)H_H\exp(-iK)$, where K is an operator changing the number of doubly occupied states [18–22]. We obtain, up to constant terms, the following spin Hamiltonian:

$$\begin{aligned} H_{\text{eff}} = {} & g^*\mu_B\mathbf{B}\cdot\sum_i \mathbf{S}_i + \sum_{i,j}\mathcal{A}^{(1)}_{i,j}\mathbf{S}_i\cdot\mathbf{S}_j + \sum_{i,\tau\neq\pm\tau'}\mathcal{A}^{(2)}_{i,\tau,\tau'}\mathbf{S}_{i+\tau}\cdot\mathbf{S}_{i+\tau'} \\ & + \sum_{i,\tau}\mathcal{A}^{(3)}_{i,\tau,-\tau}\mathbf{S}_{i+\tau}\cdot\mathbf{S}_{i-\tau} + \sum_{ijk\in\triangle}\mathcal{B}_{i,j,k}\mathbf{S}_i\cdot\mathbf{S}_j\times\mathbf{S}_k \\ & + \sum_{ijkl\in\square}\mathcal{C}_{i,j,k,l}\Bigg[\left(-\mathbf{S}_i\cdot\mathbf{S}_j+\frac{1}{4}\right)\left(-\mathbf{S}_k\cdot\mathbf{S}_l+\frac{1}{4}\right) \\ & + \left(-\mathbf{S}_j\cdot\mathbf{S}_k+\frac{1}{4}\right)\left(-\mathbf{S}_i\cdot\mathbf{S}_l+\frac{1}{4}\right) - \left(-\mathbf{S}_i\cdot\mathbf{S}_k+\frac{1}{4}\right) \\ & \times\left(-\mathbf{S}_j\cdot\mathbf{S}_l+\frac{1}{4}\right)\Bigg] + \vartheta\left(\frac{t^5}{U^4}\right), \end{aligned} \quad (5)$$

where we define the following flux-independent factors:

$$\mathcal{A}^{(1)}_{i,j} = 2\left[\frac{|t_{ij}|^2}{U(1-v)} - \frac{4|t_{ij}|^4(1+v)}{U^3(1-v)^3}\right],$$

$$\mathcal{A}^{(2)}_{i,j,k} = \frac{-4(1-2v)|t_{ij}|^2|t_{ik}|^2}{U^3(1-v)^3},$$

$$\mathcal{A}^{(3)}_{i,j,k} = \frac{2(1+v)|t_{ij}|^2|t_{ik}|^2}{U^3(1-v)^3},$$

and the following flux-dependent factors:

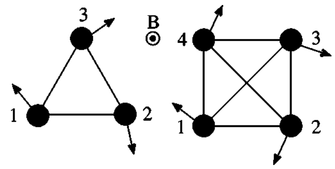

FIG. 2. Two possible looped configurations of lateral quantum dots containng single spins in a magnetic field. The triangular configuration contains three tunneling channels with one loop formed by the vertices 1231. The square configuration contains, in general, six tunneling channels with seven distinct loops formed by traversing vertices 1231, 2342, 3413, 4124, 12341, 12431, and 14231.

$$\mathcal{B}_{i,j,k} = \frac{24|t_{ij}||t_{jk}||t_{ki}|}{U^2(1-v)^2}\sin\left(\frac{2\pi\Phi_{ijk}}{\Phi_0}\right),$$

$$\mathcal{C}_{i,j,k,l} = \frac{16(5-12v)|t_{ij}||t_{jk}||t_{kl}||t_{li}|}{U^3(1-v)^2(1-3v)}\cos\left(\frac{2\pi\Phi_{ijkl}}{\Phi_0}\right).$$

The second sum in Eq. (5) contains the usual Heisenberg term if we define $J_{ij}=2|t_{ij}|^2/U$. The third and fourth sums modify the Heisenberg term and depend on the lattice vectors τ connecting a site to its neighbor. The fifth sum is a three-site sum over chiral [23] terms around distinct, closed loops ($\triangle$), denoted $\chi_{ijk}=\mathcal{B}_{i,j,k}\mathbf{S}_i\cdot\mathbf{S}_j\times\mathbf{S}_k$. The sixth sum includes four sites around distinct, closed loops ($\square$). The coefficients in the last two sums depend on the flux enclosed by three-site loops Φ_{ijk} and four-site loops Φ_{ijkl}. H_{eff} applies to any half-filled, single-band, singly occupied lattice in the presence of an external magnetic field, and in the limits $t/U \ll 1$ and $v \ll 1$.

The magnetic field dependence of the tunneling matrix elements may be calculated directly using a Wannier basis formed from dot-centered, Gaussian, single-particle states. An explicit form for $|t_{12}|^2/U$ may be found in Ref. [9] with a slightly different confinement than the one defined in Eq. (2). Reference [9] contains two results relevant for our discussion. One first observes that, in the Hubbard approximation, $|t_{12}|^2/U$ decreases exponentially with increasing magnetic field or interdot separation. Second, one finds $J_{12}\sim|t_{12}|^2/U > 0$, for all magnetic fields and interdot separations.

Equation (5) incorporates three- and four-body spin terms. The three-body chiral term splits the energy between states involving third-order virtual tunneling processes along and counter to the applied vector potential. The phase $2\pi\Phi_{ijk}/\Phi_0$ is the Aharonov-Bohm phase generated by the virtual current moving around the flux enclosed by the three-site loop. The chiral term vanishes on bipartite lattices as a result of particle-hole symmetry [22]. It plays a particularly active role in triangular lattices, Fig. 2.

While the chiral term vanishes in the zero-field limit, four-body terms survive for $N>3$. Four-body terms have been discussed in relation to coupled-quantum-dot systems in a four-site, tetrahedral geometry [10]. In the tetrahedral geometry there are three terms in the sum over four-site loops (three distinct $\square$'s) yielding a particle-exchange-symmetric, four-body contribution to the spin Hamiltonian: $\sim\Sigma_{ijkl\in\square}(\mathbf{S}_i\cdot\mathbf{S}_j)(\mathbf{S}_k\cdot\mathbf{S}_l)$. We may, similarly, consider a two-dimensional square geometry with equal tunneling between all sites. Here we find three distinct, four-site loops, Fig. 2. These add to give the term discussed in Ref. [10]. In the absence of diagonal tunneling only the exterior loop, 12341, survives, yielding the symmetry-breaking four-body term $(\mathbf{S}_1\times\mathbf{S}_2)\cdot(\mathbf{S}_3\times\mathbf{S}_4)+(\mathbf{S}_1\cdot\mathbf{S}_2)(\mathbf{S}_3\cdot\mathbf{S}_4)$, which, through $\mathcal{C}_{ijkl}$, shows flux dependence.

As the interdot separation decreases we leave the single-band, single-occupancy limit and a real current (rather than a virtual one) splits the energy spectrum. The spin splitting in this limit depends on first-order, direct-exchange processes rather than the second-order, superexchange processes discussed above. Our analysis based on the extended Hubbard model may miss qualitative features in the low-energy Hilbert space by poorly estimating the coefficients of different spin terms. Nonetheless, symmetry requires that, in the weakly-coupled-lattice limit Eq. (5) includes all possible scalars formed from spin operators, up to and including four-body terms. While the magnitude of these coefficients may be estimated accurately by expanding the Hilbert space, we seek to study the qualitative physics associated with changes in sign. To go beyond our single-band lattice model we account for qualitative changes in sign by modeling orbital effects with a variational ansatz.

B. Variational states

We now discuss a set of variational states which model the low-energy orbital states of Eq. (1) in an effort to go beyond the Hubbard limit discussed above. To obtain an accurate variational wave function we examine the form of the exact wave function in two limits: the upper left and lower right corners of Fig. 1. We then construct an ansatz that connects both regimes. We begin with the simplest system $N=2$. It is analytically soluble in two extreme regimes: Two well-separated one-electron "artificial atoms" and a two-electron artificial atom in a high magnetic field. The first case is trivial and consists of two well-separated quantum dots (akin to two well-separated one-electron atoms *not* in a molecular state) with one electron in each dot, $R/a \gg 1$. In this case we may ignore the Coulomb interaction. The noninteracting ground state consists of degenerate singlet and triplet states.

In the second soluble limit (a two-electron artificial atom) two electrons lie in one parabolic dot in a strong magnetic field. In this case we take $\omega_c/\omega_0 \gg 1$ and $R=0$. Correspondingly, the relative and z component of the angular momentum commute with the Hamiltonian. At large magnetic fields we may project Eq. (1) onto the lowest Landau level (LLL), giving

$$H|_{\omega_0 \ll \omega_c, R=0} = \gamma\hat{L}_z + \sum_{m=0}^{\infty}\mathcal{V}_m\hat{P}_m, \tag{6}$$

where we define $\gamma\equiv(\hbar/2)(\sqrt{\omega_c^2+4\omega_0^2}-\omega_c)$ and $\hat{L}_z$ is the total angular momentum in the z direction. The second term represents the LLL Coulomb interaction, projected onto eigenstates of relative angular momentum m via the projection operator $\hat{P}_m$. The coefficients $\mathcal{V}_m$ are the Haldane pseudopotentials [24] which, for the Coulomb interaction, decrease with increasing m, at large m. The unnormalized eigenstates of relative angular momentum are

$$|m\rangle = (z_1 - z_2)^m \exp\left(\frac{-|z_1|^2 - |z_2|^2}{4a^2}\right), \qquad (7)$$

where $z=x+iy$. It can be shown directly that, because there is no center-of-mass motion, the above wave functions are also eigenstates of $\hat{L}_z$, with eigenvalue m. Thus the set of states $|m\rangle$ form an orthogonal set of eigenstates of Eq. (6), with eigenvalues $E_m=\gamma m+\mathcal{V}_m$. The relative angular momentum of the lowest energy state depends on the parameters in γ and the form of the interaction. For the LLL Coulomb interaction, in the artificial zero-field limit, the lowest energy state has $m=1$. Increasing B lowers the confinement energy cost $\gamma m \sim m/B$, and raises the Coulomb cost $\mathcal{V}_m \sim \sqrt{B/(m+1)}$, thereby raising m by 1. The transition from one eigenstate to the next occurs when $E_m=E_{m+1}$ which, for $\omega_c/\omega_0 \gg 1$, occurs at magnetic fields

$$B_m \approx \left(\frac{C}{\tilde{\mathcal{V}}_m - \tilde{\mathcal{V}}_{m+1}}\right)^{2/3}, \qquad (8)$$

where $\tilde{\mathcal{V}}_m \equiv \mathcal{V}_m/(e^2/4\pi\varepsilon a)$ and $C\equiv 4\pi\varepsilon\hbar^{3/2}\omega_0^2 m^* e^{-7/2}$. For $\hbar\omega_0=3$ meV we find $C[\mathrm{T}^{3/2}]\sim 1.2$. The states $|m\rangle$ are symmetric (antisymmetric) with respect to particle exchange if m is even (odd). The total wave function $\mathcal{A}[|\psi\rangle \otimes |\lambda\rangle_2]$ must be antisymmetric. Therefore $|\lambda\rangle_2$ is spin singlet (triplet) for m even (odd). Here, the index m may be interpreted as the number of zeros or vortices attached to each electron, allowing us to assign a vorticity to each spin state.

We now construct variational states which reproduce the exact results discussed above and the low-energy physics of the intermediate, physical parameter regime as well, $R/a \sim 1$ and $\omega_c/\omega_0 \sim 1$. The composite fermion theory [25] of the fractional quantum Hall effect offers an accurate variational ansatz describing two-dimensional electron systems at high magnetic fields. A composite fermion is the bound state of an electron and an even number of quantum-mechanical vortices of the many-body wave function. The corresponding orbital wave function is [17,25] $\psi=\mathcal{J}\phi$, where ϕ is a weakly interacting fermion state, $\mathcal{J}$ a Jastrow factor, and ψ the highly correlated state of electrons. In isotropic, spinless systems $\mathcal{J}$ attaches an even number of vortices to the fermions in the antisymmetric state ϕ yielding an antisymmetric electron wave function. In anisotropic systems with additional quantum numbers one may bind an even *or* odd number of vortices to each particle while preserving the antisymmetry of the overall wave function [26,27]. Applying the composite fermion ansatz to the Hamiltonian studied here we take ϕ to be the noninteracting ground state of Eq. (1). A more rigorous, but technically demanding, approach for large systems should use the weakly interacting ground state instead. We also take $\mathcal{J}=\Pi_{j<k}(z_j-z_k)^p$, where $p=0,1,2,\ldots$, giving

$$\overline{\psi_p} = \prod_{j<k} (z_j - z_k)^p \phi. \qquad (9)$$

This is our initial, high-field solution of Eq. (1) at arbitrary N. $\overline{\psi_p}$ reduces to Eq. (7) at $R=0$. For $R/a \gg 1$ the fermions in the state ϕ become localized on each dot leaving $\mathcal{J}$ constant $\sim R^p$, in which case $\overline{\psi_p}$ reduces to the limit of two independent electrons.

To improve the variational states in the low-field regime, $\omega_c/\omega_0 \leqslant 1$, we note that the Coulomb energy cost may be lowered by mixing with higher energy states of the quantum dot thereby increasing the average interelectron separation. In the $R=0$ limit, rotational symmetry requires the addition of states with the same angular momentum. This leads to the following trial states:

$$\psi_p = \prod_{j<k} (z_j - z_k)^p (1 + \beta b^\dagger a^\dagger)\phi, \qquad (10)$$

where the variational parameter β controls the amount of mixing with higher energy levels of the quantum dot. The total raising operators $b^\dagger=b_1^\dagger+\cdots+b_N^\dagger$ and $a^\dagger=a_1^\dagger+\cdots+a_N^\dagger$ act on the Fock-Darwin basis states centered between the dots. The single-particle raising operators are given by $b_j^\dagger=(z_j^*/2-2\partial_{z_j})/\sqrt{2}$ and $a_j^\dagger=i(z_j/2-2\partial_{z_j^*})/\sqrt{2}$. The above variational states include mixing with higher-energy states of the same angular momentum because the operator $b^\dagger a^\dagger$ does not change the angular momentum of a Fock-Darwin state. They will be tested in Sec. IV.

III. SPIN-BASED QUANTUM DOT QUANTUM BITS

Gate operations on single and multispin qubits rely on the adiabatic evolution of the spin state under the unitary time evolution operator defined in terms of the appropriate spin Hamiltonian [e.g., Eq. (5)]:

$$\mathcal{T}\exp\left(-i\int_0^T H_{\mathrm{eff}}(t)dt\right)|\lambda(t'=0)\rangle_N, \qquad (11)$$

where $\mathcal{T}$ indicates time ordering and T the duration of a gate pulse. The qualitative spin physics captured by the spin Hamiltonian, Eq. (5), therefore plays a crucial role in defining gates formed from coupled quantum dots. Concurrently, the orbital states Eq. (10) can be used to calculate the parameters in Eq. (5) and their regime of applicability. In forming quantum gates out of coupled, single-spin quantum dots we study modifications to the Heisenberg paradigm and its implications for qubit proposals in three different systems: (A) two strongly coupled quantum dots; (B) three simultaneously weakly coupled quantum dots, and (C) four simultaneously weakly coupled quantum dots.

A. Two quantum dots

Solid-state qubit proposals often make use of the Heisenberg exchange interaction between spins in neighboring quantum dots. The exchange interaction offers the potential for a universal set of quantum gates through the adiabatic operation of the exchange gate with [1] or without [14] single-spin operations. Application of the exchange gate to the two-dot system will be an adiabatic process if the energy between the lowest, unwanted excited state of the double quantum dot and the highest spin state storing quantum information is much larger than the exchange splitting, $\Delta \gg J_{ij}$. This condition is satisfied in the spin Hamiltonian regime in Fig. 1 but is not necessarily met if we change the parameters in Eq. (1) slightly because J has exponential B and R dependence at large B and R, respectively [9]. In fact, experiments on coupled quantum dots, while pushing for shorter gate times (and hence larger exchange energies) may indeed leave the border defined by the solid line in Fig. 1 [9,28]. It is therefore important to understand the low-energy Hilbert space of the coupled-dot system when $J_{ij} \gtrsim \Delta$. We will show, for $N=2$, that the variational states discussed in Sec. II B capture the magnetic field dependence of Δ. At large fields the variational states describe a bound state between electrons and vortices of the N-body wave function. We find the smallest Δ, $\Delta_{\min}$, to occur when the vorticity (the number of vortices attached to each electron) of the first excited states mix to form an anticrossing.

B. Three quantum dots

An accurate characterization of the double-dot system allows us to define the appropriate parameter regime in which to study several Heisenberg coupled quantum dots and associated magnetic field effects. Two spin states of a three-quantum-dot structure can serve as an encoded qubit. We first construct encodings which protect quantum information stored in many-body spin states. These encodings assume a noise operator which, as a demonstration, we choose to be collective or Zeeman-like. We then search for degeneracies in the set of states generated by these noise operators. The $S=1/2$ sector of the $N=3$ system provides a simple example of a quantum-dot decoherence-free subsystem [29,30]. Consider three electrons confined to three quantum dots whose centers lie at the vertices of an equilateral triangle as shown schematically in Fig. 2. In this case a decoherence-free subsystem makes use of a fourfold degeneracy at $B=0$ to protect quantum information stored in the qubit defined by $|\lambda\rangle_3$, where $\lambda=0$ or 1, from fluctuations in the Zeeman energy. The four states are [31]

$$|\lambda\rangle_3 \otimes |-1/2\rangle = \frac{-1}{\sqrt{3}}(|\downarrow\downarrow\uparrow\rangle + \omega^{\lambda+1}|\downarrow\uparrow\downarrow\rangle + \omega^{2-\lambda}|\uparrow\downarrow\downarrow\rangle),$$

$$|\lambda|_3 \otimes |+1/2\rangle = \frac{1}{\sqrt{3}}(|\uparrow\uparrow\downarrow\rangle + \omega^{\lambda+1}|\uparrow\downarrow\uparrow\rangle + \omega^{2-\lambda}|\downarrow\uparrow\uparrow\rangle), \tag{12}$$

where $\omega \equiv \exp(2\pi i/3)$. The second term in the tensor product denotes the total z component of spin.

Up to second order, Eq. (5) allows an encoding against Zeeman-like or collective noise. By collective noise we mean an interaction between spins and the environment which acts the same on all spins. By construction, the Zeeman term may alter the energy difference between the states in Eq. (12) with different S_z, but not λ. However, the chiral term in Eq. (5) acts *noncollectively*. The chiral and Zeeman terms remove all degeneracies required to construct a qubit immune to fluctuations in the perpendicular magnetic field. Explicitly,

$$\chi_{123}|\lambda\rangle_3 = \frac{\mathcal{B}_{123}}{4}(2\lambda-1)\sqrt{3}|\lambda\rangle_3, \tag{13}$$

where $\mathcal{B}_{123}=(12tJ/U)\sin(2\pi\Phi_{123}/\Phi_0)$ in the case $J_{ij}=J$ and $|t_{ij}|=t$ for all i and j.

Following Ref. [32] we may now, using Eq. (5), construct a projected spin Hamiltonian which acts on the encoded basis states $|\lambda\rangle_3$:

$$\overline{H}_{N=3} = \mathbf{F}_3(\mathcal{A}^{(1)},\mathcal{A}^{(2)},\mathcal{A}^{(3)}) \cdot \overline{\mathbf{S}} + \frac{\sqrt{3}}{2}\mathcal{B}_{123}\overline{S_z}, \tag{14}$$

where $\overline{\mathbf{S}}$ is a pseudospin operator defined by projection onto two encoded basis states, $|\lambda\rangle_N$ in our case. $\mathbf{F}_N$ is a basis-dependent effective magnetic field which may be tuned through suitable manipulation of t_{ij} and depends *only* on the coefficients of the two-body terms in Eq. (5). $\mathbf{F}_N$ may be calculated from these two-body terms using the exchange operator: $E_{ij}=(4\mathbf{S}_i\cdot\mathbf{S}_j+I_{ij})/2$, where I is the identity operator. As is apparent from Eq. (14), χ_{123} yields an *effective* Zeeman splitting between the encoded basis states of the three-spin qubit. In Sec. IV B we verify numerically that the chiral term is actually sizable in the spin Hamiltonian regime of Fig. 1. We therefore arrive at a revealing inconsistency in seeking a decoherence-free subsystem from a looped, three-spin system. Part of our motivation for simultaneously coupling three spins was to remove the Zeeman term as a potential noise source. However, we have only enhanced the system's dependence on the external magnetic field by coupling the three spins in a loop.

In the event that we may control the flux through the three-spin system, the chiral term offers an additional one-qubit gate. This term yields two advantages. The first stems from a comparison with single-spin operations using localized magnetic fields. The three-spin object encompasses a larger area than a single spin and therefore eases constraints on locally applied magnetic fields used in applying single-spin gates. Second, exchange-only encoded universality schemes require a large overhead and extremely accurate application of the exchange gate to implement elementary algorithms. The chiral term may offer some relief form these constraints using algorithms which include the new, encoded Pauli-Z gate in Eq. (14).

C. Four quantum dots

We now turn to the case of four coupled spins, the lowest number of physical spins supporting a decoherence-free subspace [33,34]. We begin with four quantum dots containing four electrons coupled with equal tunneling $|t_{ij}|=t$, including diagonal terms. Figure 2 shows a two-dimensional schematic. With equal tunneling we find a decoherence-free subspace among two $S=0$ states corresponding to $\lambda=0$ and 1:

$$|\lambda\rangle_4 = |\uparrow\uparrow\downarrow\downarrow\rangle + |\downarrow\downarrow\uparrow\uparrow\rangle + \omega^{\lambda+1}|\uparrow\downarrow\uparrow\downarrow\rangle + \omega^{\lambda+1}|\downarrow\uparrow\downarrow\uparrow\rangle + \omega^{2-\lambda}|\downarrow\uparrow\uparrow\downarrow\rangle + \omega^{2-\lambda}|\uparrow\downarrow\downarrow\uparrow\rangle. \quad (15)$$

Including all single- and two-body-spin terms in Eq. (5), these states show no explicit magnetic field dependence (excluding the magnetic field dependence of $|t_{ij}|$ discussed in Sec. II A). As for the three-body term, the spin Hamiltonian must respect the intersite exchange symmetry inherent in the lattice. In the basis $|\lambda\rangle_4$ we find

$$\sum_{ijk\in\triangle} \chi_{ijk} \otimes I_l |\lambda\rangle_4 = \frac{\sqrt{3}}{4}(2\lambda - 1) \sum_{ijk\in\triangle} \mathcal{B}_{ijk}\epsilon_{ijkl}|\lambda\rangle_4, \quad (16)$$

where ϵ_{ijkl} is the four-component Levi-Cività symbol and the sum excludes $l=i$, j, or k. As expected, the sum vanishes with tunneling $|t_{ij}|=t$ for all i and j even in a uniform, external magnetic field.

Four-spin terms have a simple representation in the $|\lambda|_4$ basis. The last sum in Eq. (5), in the case $|t_{ij}|=t$, involves three sums over four-site loops. Writing the four-spin terms with the exchange operator, we find that they act as the identity operator in the basis defined by $|\lambda|_4$. In this case we have a simple, projected Hamiltonian:

$$\overline{H}_{N=4} = \mathbf{F}_4(\mathcal{A}^{(1)},\mathcal{A}^{(2)},\mathcal{A}^{(3)}) \cdot \overline{\mathbf{S}}. \quad (17)$$

It is important to note that $\mathbf{F}_4$ depends only on coefficients from two-body spin terms of the form $\mathbf{S}_i \cdot \mathbf{S}_j$. The three- *and* four-body spin terms (and therefore external sources of flux through closed loops) do not affect the symmetric four-dot structure with diagonal tunneling. They must maintain intersite exchange symmetry imposed by the lattice, precisely the symmetry exploited in constructing the decoherence-free subspace $|\lambda|_4$.

We now consider symmetry-breaking effects. In the absence of diagonal tunneling ($t_{i,i+2}=0$) only the external loop, around vertices 12341 in Fig. 2, in the last sum of Eq. (5) survives. The external loop alone breaks particle-exchange symmetry. The additional term can be written $(\mathbf{S}_1 \times \mathbf{S}_2)\cdot(\mathbf{S}_3 \times \mathbf{S}_4)+(\mathbf{S}_1\cdot\mathbf{S}_2)(\mathbf{S}_3\cdot\mathbf{S}_4)$, excluding two-body spin terms. The entire looped term, including two-body spin terms, contributes the following term to $\overline{H}_{N=4}$: $-\mathcal{C}_{1234}(\overline{S}_x+\sqrt{3}\overline{S}_y)$. From this term we see that in the square geometry fourth-order terms not only modify the Heisenberg interaction, and hence the effective magnetic field $\mathbf{F}_4$, but also add an effective in-plane field in the $|\lambda|_4$ basis. The size of this effective in-plane field depends on the real external flux piercing the square plaquette through $\mathcal{C}_{1234} \sim \cos(2\pi\Phi_{1234}/\Phi_0)$.

Additional symmetry breaking occurs during gate pulses crucial to encoded universality schemes. In order to implement Pauli gating sequences on the encoded four-spin qubit we must tune $\mathbf{F}_4$ and therefore the tunneling matrix elements t_{ij}. When applied to a decoherence-free subspace an encoded Pauli gate composed of Heisenberg terms must, by construction, involve a spin-specific asymmetry. An example was considered in Ref. [15]: $|t_{31}|=|t_{23}|=|t_{34}|=t(1+\delta)$, where δ is a number and all other $|t_{ij}|=t$. The sum over chiral terms in Eq. (16) then induces an energy splitting $24\pi\sqrt{3}tJ\delta AB_z/(U\Phi_0)$ between the states with $\lambda=0$ and 1 for

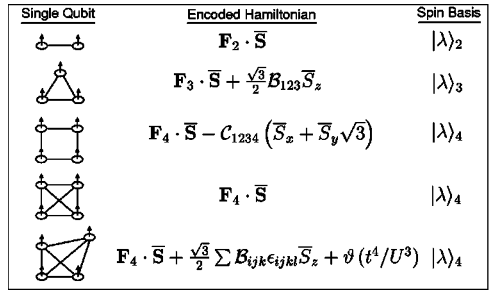

FIG. 3. Table showing possible multispin qubits in the left column, the encoded Hamiltonian in the center column, and the corresponding two-state basis in the right column. In the left column arrows denote single spins while lines indicate tunneling channels which are all equal except in the last row. The Hamiltonians in the center column are written in terms of the encoded spin $\overline{\mathbf{S}}$ defined via the two encoded basis states $|\lambda|_N$. For $N=2$ the basis states are the $S_z=0$ singlet and triplet states while for $N=3$ and 4, $|\lambda|_N$ is defined in Eqs. (12) and (15), respectively. The effective magnetic fields $\mathbf{F}_N$ depend only on the coefficients of two-spin Heisenberg terms, $\mathcal{A}^{(i)}$, in Eq. (5). The factors $\mathcal{B}$ and $\mathcal{C}$ depend on the coefficients of three- and four-spin terms in Eq. (5) and therefore the flux through closed loops.

$\Phi_{ijk}/\Phi_0 \ll 1$. Here A is the area of the triangle defined by the vertices 123 in the square geometry of Fig. 2. This configuration is depicted in the last row of Fig. 3. The table summarizes five-spin-cluster qubit configurations and their encoded Hamiltonians written in the $|\lambda|_N$ basis. From the table we see that configurations which break intersite symmetry (rows 2, 3, and 5) have non-Heisenberg terms which depend on the flux through closed loops.

IV. NUMERICAL RESULTS AND DISCUSSION

The accuracy of our perturbative and variational analyses may be checked numerically. We study two systems in particular, two electrons in two adjacent quantum dots and three electrons in three adjacent quantum dots arranged in a triangle. We diagonalize the full Hamiltonian Eq. (1) in several regimes, including $R/a \sim 1$ and $\omega_c/\omega_0 \gtrsim 1$. We construct the matrix representing H in the Fock-Darwin [35] basis centered between the dots. Previous studies have employed diagonalization of similar Hamiltonians using several dot-centered basis states. This technique requires lengthy numerical routines to generate an orthogonal set of Wannier basis states [9,39]. The limited number of Wannier basis states allows for high accuracy only in a regime where the Coulomb interaction may be treated perturbatively. However, in our treatment we are able to access the strongly correlated regime by including up to $\sim 10^5$ Fock-Darwin basis states with z component of angular momentum less than 12. We use a modified Lanczos routine to obtain the ground and excited states. This technique yields the *entire* spectrum. However, here we focus on the lowest energy states. The energies for $N=2$ converge to within 1 μeV upon inclusion of more basis states and may therefore be considered exact. While, for the $N=3$ system, the ground- and excited-state energies converge to within 6 μeV upon inclusion of more

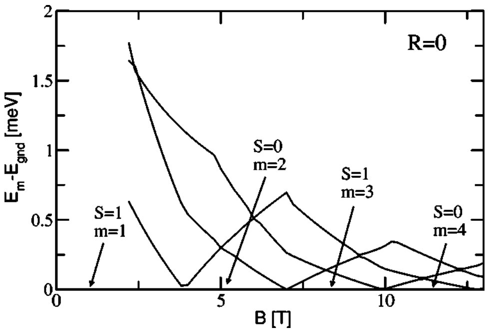

FIG. 4. Energy of the four lowest states of a single quantum dot ($R=0$) with two electrons under a perpendicular magnetic field in the lowest Landau level plotted as a function of perpendicular magnetic field. The ground-state energy is set to zero and the parabolic confinement parameter is $\hbar\omega_0=3$ meV. The ground state, with orbital wave function given by Eq. (7), alternates between spin singlet ($S=0$) and triplet ($S=1$) as a function of magnetic field. The spin singlet and triplet states correspond to even and odd angular momentum quantum numbers m, respectively.

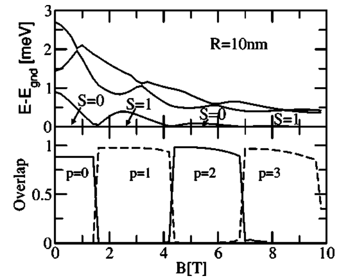

FIG. 5. The top panel plots the energy of the four lowest states of Eq. (1) obtained by exact diagonalization as a function of magnetic field with the ground-state energy set to zero. The separation between parabolic dots is now $R=10$ nm. The parabolic confinement parameters is $\hbar\omega_0=3$ meV. Transitions between spin singlet and triplet states remain. The bottom panel shows the overlap of the exact ground state and the trial states given by Eq. (9). The number of vortices attached to each electron increases with magnetic field from $p=0$ to 3. As in Fig. 4, singlet (triplet) states correspond to even (odd) values of p.

basis states giving a strict variational bound to the accuracy. However, the slow convergence is due to corrections in the overall confinement energy cost, $\sim$10 meV. The energy differences quoted here converge much faster (<2 μeV) as we increase the number of basis states and may therefore be considered exact, with a few exceptions. These exceptions occur near degeneracy points where our Lanczos routine requires a prohibitive number of steps to distinguish between two states whose energies are within 5 μeV of each other. In these rare, but important, cases we extrapolate between the nearest convergent energies.

A. Two quantum dots

We seek a quantitatively accurate description of the boundaries and underlying physics of all regions depicted in Fig. 1. While we find that the perturbative expansion in Sec. II A is valid for $R/a>1$ and $\omega_c/\omega_0 \lesssim 3$, the remaining portions of the parameter space involve long-range correlations. Using the $N=2$ system we check the accuracy of the variational ansatz discussed in Sec. II B in several limits. We expect that the variational states discussed there should remain valid for $N>2$, with appropriate modifications.

We begin with the $R=0$, lowest-Landau-level limit discussed at the beginning of Sec. II B. The LLL approximation cleanly brings out the physics behind the high-field spin transitions in two-electron quantum dots but, as we have discussed, needs modification at low magnetic fields. Figure 4 plots E_m-E_{gnd} versus B for the four lowest energy states $m=1$, 2, 3, and 4 with $S_z=0$. The parabolic confinement parameter is $\hbar\omega_0=3$ meV. Cusps appear at $E_m-E_{\mathrm{gnd}}=0$ where the ground state changes at B_m signaling a change in the number of vortices per electron. [Note that the relation for B_m, Eq. (8), is valid for $\omega_c/\omega_0 \gg 1$.] The ground state clearly shows a number of spin transitions with increasing magnetic field [36]. Furthermore, the second-highest excited state becomes degenerate with the third at level crossings which occur at magnetic fields between ground-state transitions. This suggests that quantum information stored in the two lowest energy spin states in neighboring quantum dots becomes susceptible to leakage when the dots are brought very close together.

We now turn to the case with finite interdot separation $R>0$ outside of the LLL. The top panel in Fig. 5 shows the four lowest energies obtained from exact diagonalization of Eq. (1) versus magnetic field. The energy zero is taken to be the ground state. We have chosen an interdot separation of $R=10$ nm, confinement $\hbar\omega_0=3$ meV, and $S_z=0$. The energy of the first excited state gives the effective exchange splitting which changes sign through successive spin transitions at each cusp. The results are qualitatively similar to the results shown in Fig. 4 but are entirely unexpected. Vortex attachment nonperturbatively lowers the Coulomb energy of uniform states but does not necessarily apply to highly disordered systems. Yet the intriguing oscillations in the effective exchange interaction seen in Fig. 5 suggest just this and therefore require further study.

In comparing Figs. 4 and 5 we find further differences. At low fields, the top panel of Fig. 5 correctly shows a spin singlet ground state at $B=0$ rather than a triplet state as shown in the unphysical, LLL limit of Fig. 4. Most importantly, the degeneracies in excited states at $B=0$, 2.4, 5.2, and 8 T begin to lift, giving $\Delta_{\min}>J$. As opposed to the level crossing in the single-dot $R=0$ case discussed earlier, the breaking of rotational symmetry forces an anticrossing among the first and second excited states. At small to intermediate interdot separations $R/a \lesssim 1$, the higher excited states are perturbed single-dot states with a nearly uniform charge density.

A large anticrossing among the two lowest excited states protects the quantum information stored in the entangled state of two strongly coupled quantum dots. Experimental uncertainties in R and ω_0 may eventually lead to the strongly coupled regime. Careful study of the states making up the anticrossing is therefore crucial. The bottom panel of Fig. 5 plots the overlap of the exact ground state and the variational state Eq. (9) at $R=10$ nm. Triplet (singlet) spin states corre-

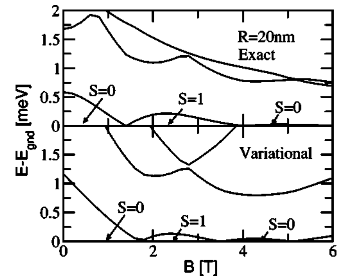

FIG. 6. The top panel shows the same as Fig. 5 but for a dot separation of $R=20$ nm. The bottom panel shows the energy of the trial states in Eq. (10) as a function of magnetic field. The ground-state energy is set to zero. The energies are obtained by orthogonalizing the four modified variational states with $p=0$, 1, 2, and 3 and diagonalizing Eq. (1). The variational parameter β is chosen to minimize the total energy.

spond to odd (even) values of p, as in the $R=0$ case. The overlaps drop to zero when the particle-exchange symmetry of the orbital wave function changes. We have checked by direct calculation of the density that, by $B\sim 9$ T, the modified magnetic length has become small enough to localize the electrons on each dot. The surprisingly high overlaps prove that vortex attachment is a valid ansatz even in the highly localized regime. At large dot separations $R\geqslant 40$ nm, the Coulomb interaction lowers to a point where the splitting between spin states is near zero at large B. However, we have checked that even here the overlaps remain large. Another important feature of Eq. (9) is that the $p=0$ state does not take into account the Coulomb interaction. The overlaps near $B=0$ are correspondingly lower.

The top panel in Fig. 6 plots the exact energy spectrum, as in Fig. 5, but for $R=20$ nm. Here we see that, at large magnetic fields, the large separation between electrons localized on each dot suppresses the exchange splitting. However, several spin transitions still remain. The bottom panel in Fig. 6 shows the energy of the four variational states Eq. (10) with $p=0$, 1, 2, and 3. We take the ground state to be the zero in energy. We obtain the energy by orthogonalizing the four variational states and diagonalizing Eq. (1) in this four-state basis. These variational states are an improvement over Eq. (9). They include mixing with higher energy levels of the dots. The mixing is tuned with the variational parameter β. We minimize the energy with respect to β at each B. The parameter β of the ground state varies from 0.02 at $B=0$ to 0.0006 at $B=5$ T, showing that large magnetic fields all but suppress Landau level mixing. The exchange splitting obtained with the variational states compares well with the exact value. Furthermore, in the range $B=1-4$ T, the second excited state captures the essential features of the corresponding exact results. Rotational symmetry breaking forces the higher excited states to open an anticrossing observed near $B=0$, 2.4, and 4.3 T. The states at the anticrossings in Fig. 6 are similar to the states making up the level crossings in Fig. 4. For example the electrons in the first excited state at 2.4 T in Fig. 6 form a two- and zero-vortex mixed state in a 56% to 44% ratio, as opposed to the ground state which holds one vortex per electron, to within 98%. To evaluate the anticrossing explicitly we note that for $R/a\ll 1$ the asymmetry in confinement acts as a perturbation. We may rewrite the confinement potential up to an overall constant:

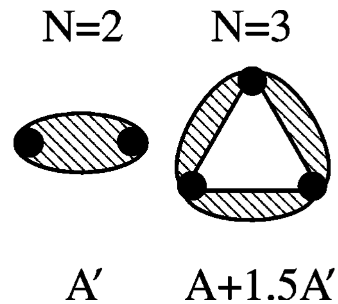

FIG. 7. Schematic diagram showing the area enclosing flux in the $N=2$ and 3 systems defined by the density of the N-body ground state. The dots represent the centers of the parabolic quantum dots. The patterned region for the $N=2$ system defines an area A' symmetric about the axis joining the two dots. For the $N=3$ system the triangular region encloses an area A. A correction to the triangular region, shown by the three patterned additions, defines an area $\approx 3A'/2$.

$$V_{N=2}(\mathbf{r}) = \frac{m^*\omega_0^2}{2}(|\mathbf{r}|^2 - |x|R). \tag{18}$$

The second term breaks rotational symmetry and forces an anticrossing among the lowest two excited states. It is important to note that the two lowest excited states involve states of even vorticity. Symmetry allows these two states to mix, yielding an anticrossing, as one may find by diagonalizing the rotational symmetry-breaking term in the even-vorticity subspace. The matrix elements are $m^*\omega_0^2 R/2\langle\psi_{p'}\|x_1| + |x_2\|\psi_p\rangle$, where, near $B=2.4$ T for example, p and p' may be 0 or 2. These matrix elements give an anticrossing $\Delta_{\min} \sim m^*\omega_0^2 Ra + J$. This is in contrast to ground-state transitions between states with even and odd vorticity. Here the states ψ_p and ψ_{p+1} cannot mix, allowing the exchange splitting to change sign.

We stress that the top panel in Fig. 6 is obtained by diagonalization of Eq. (1) with $\sim 10^5$ basis states while the lower panel is obtained by the same method but with four physically relevant basis states. The agreement breaks down at larger fields, $B\sim 5.6$ T, because we have not included the $p=4$ variational state in the excited states. Inclusion of variational states with large p is necessary at larger fields. The excellent agreement obtained thus far demonstrates that the plethora of spin transitions in strongly coupled double quantum dots originates from a swapping of the particle-exchange symmetry associated with vortex attachment.

We may parametrize the high-field effects of vortex attachment in an effective spin Hamiltonian based on the above numerical results and our analysis in Sec. II B. Note that the exchange interaction changes sign in a roughly periodic fashion as each electron captures an additional vortex. The vortex may be interpreted, by equating its Berry's phase [37] to an Aharonov-Bohm phase, as additional flux [25]. The confinement, determined by ω_0, fixes the area defined by the electronic wave function. A', depicted schematically by the patterned region on the $N=2$ side of Fig. 7. From Fig. 5

we note that we may count the number of vortices attached to each electron using the flux through the double-dot system, BA'/Φ_0. The parameter A' is fixed by requiring that the net Berry's phase swept out by one quasiparticle (the electron plus the attached vortices) circling the other quasiparticle as it encloses the double-dot system, $2\pi[BA'/\Phi_0-(N-1)p]$, must vanish for $p=2$ [38]. The net flux includes the effective flux due to the Berry's phase associated with attaching p vortices to each electron. The data in Fig. 5, for example, show that at $B=5.4$ T the flux through the double-dot system exactly cancels the effective flux due to the attached vortices (two for each electron). By fixing A' in this way, $\pi BA'/\Phi_0$ increases by integer multiples of π as each electron captures an additional vortex. We may then write a parametrized spin Hamiltonian (up to second order in t^2/U)

$$H_{\text{eff}}^{(2)} = 2\tilde{J}_{12}\mathbf{S}_1 \cdot \mathbf{S}_2, \tag{19}$$

where $\tilde{J}_{12} \sim (2t^2/U)\cos(\pi BA'/\Phi_0)$. We determine A' from our numerical data and set $t=|t_{12}|$. We have, for simplicity, excluded the Zeeman term. From Fig. 5, for example, we find the center of the $p=2$ region to be $\Phi_0/A' \approx 5.4$ T which gives $A' \sim 800$ nm^2. The parameter A' suggests confinement of an appreciable part of the single-electron density to within a radius of ~ 10 nm. When we insert the magnetic field dependence [9] of $|t|$ and U into $H_{\text{eff}}^{(2)}$ we obtain qualitative agreement with our numerical estimates of J_{ij} at all magnetic fields. But, without the cosine term, t^2/U remains positive for all B.

B. Three quantum dots

We now study the $N=3$ system where the quantum dots lie at the vertices of an equilateral triangle with side lengths $R=40$ nm [15]. We know from the previous section that a large interdot separation will prevent unwanted excited states of the quantum dot from approaching the spin states defining our qubit. We further expect the analysis of Sec. II A to hold only for low magnetic fields while, at large fields, electrons capture vortices and initiate spin transitions. As a consequence, an external magnetic field has three noticeable effects. (1) At low fields the length scale a is set by confinement and the flux enclosed by the triangular loop will dominate the magnetic field dependence of the states in Eq. (12). (2) At higher fields the length scale shrinks with increasing magnetic field. The interdot tunneling matrix elements will be suppressed as the electrons become more localized on each dot. (3) The electrons will simultaneously capture vortices to screen the increased Coulomb interaction. The latter effect, as for the $N=2$ system, should, in the appropriate parameter regime, lead to oscillations in the total spin of the ground state as a function of magnetic field.

Figure 8 shows the energy of the lowest states obtained from exact diagonalization of H in the $S_z=1/2$ sector as a function of magnetic field. The confinement parameter is taken to be $\hbar\omega_0=6$ meV for the top panel and 3 meV for the bottom panel. The energy of the state $|\lambda=0\rangle_3$ is set to zero. At $B=0$ the two lowest energy states have total spin $S=1/2$ and are degenerate, as expected from the reflection symmetry of the triangular confining potential. The next highest state has $S=3/2$ which corresponds to $6|t_{ij}|^2/U \approx 0.13$ meV. Above this state we find (not shown) the higher excited states to lie above 1 meV.

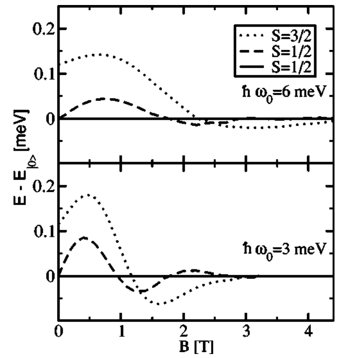

FIG. 8. Energy of the three lowest energy states versus perpendicular magnetic field obtained from exact diagonalization of Eq. (1) in the $S_z=1/2$ sector for $N=3$. The centers of the lateral parabolic quantum dots lie at the vertices of an equilateral triangle with 40 nm side lengths. The dotted line has total spin $S=3/2$ while the dashed ($|\lambda=1\rangle_3$) and solid lines ($|\lambda=0\rangle_3$) have $S=1/2$. The energy of the $S=1/2$ state corresponding to $|0\rangle_3$ is set to zero. The top panel has a parabolic confinement parameter $\hbar\omega_0=6$ meV while the bottom panel has $\hbar\omega_0=3$ meV. The change in confinement changes the effective area of the system and, as a consequence, the position of degeneracy points between $B=1$ and 3 T.

We focus first on the low-magnetic-field data. As we increase the magnetic field the magnetic vector potential breaks the symmetry of the confining potential leading to a splitting between the two lowest states. The splitting is linear in B, for small B, as in Eq. (13). We expect such a simple behavior because the two-body terms in Eq. (5) have weak magnetic field dependence at low magnetic fields, through $|t_{ij}|^2/U$. Alternatively, the chiral term annihilates $S=3/2$ states. Only two-body terms in Eq. (5) affect the $S=3/2$ state. We therefore expect that the energy of the $S=3/2$ state, $E_{S=3/2}$, decreases very slowly with increasing magnetic field at low fields (while $E_{S=3/2}-E_{|0\rangle_3}$ should increase linearly). Here the contribution from the chiral term is sizable and is, for the parameters studied here, larger than the Zeeman splitting of a single spin in GaAs, $\approx 0.025B[T]$ meV.

We now turn to the high-field effects in Fig. 8. For highly localized, noninteracting particles we expect the flux in $\mathcal{B}_{123}$ to be BA/Φ_0, where A is simply the the area of the triangle defined by the centers of the three quantum dots. However, in our system, the parabolic confinement will not perfectly localize the interacting electrons. The area swept out by a closed loop around the bulk of the wave function will enclose an area larger than the triangle. Figure 7 shows a schematic representation of the new, larger area encompassed by the $N=3$ system. The additional area due to the expansion of the wave function is $\approx 3A'/2$, where A' is the area enclosed by an equivalent $N=2$ system. We may use our analysis from the previous section to determine the area added to the triangle. The net Berry's phase associated with virtual tunneling processes of quasiparticles around the $N=3$ system will be

$$2\pi\left(\frac{BA}{\Phi_0}+\frac{3BA'}{2\Phi_0}-(N-1)p\right). \tag{20}$$

The additional flux will appear in the flux-dependent factors in Eq. (5). We rewrite the three-spin Hamiltonian in the case of equal tunneling t (excluding the Zeeman, extended Hubbard, and fourth-order terms):

$$H_{\mathrm{eff}}^{(3)}=\widetilde{J}\sum_{i,j}\mathbf{S}_i\cdot\mathbf{S}_j+\frac{24t^3}{U^2}\sin\left(\frac{2\pi\Phi_{(3)}}{\Phi_0}\right)\mathbf{S}_1\cdot\mathbf{S}_2\times\mathbf{S}_3, \tag{21}$$

where $\widetilde{J}\sim(2t^2/U)\cos(\pi\Phi_{(2)}/\Phi_0)$. We define $\Phi_{(2)}=BA'$ and $\Phi_{(3)}\approx B(A+3A'/2)$. Note that the integer p, in Eq. (20), does not contribute to the chiral term. Therefore, vortex attachment does not directly affect the flux in the chiral term. Furthermore, the cosine in the first term parametrizes large-magnetic-field behavior while the sine in the second, chiral term, was derived using perturbation theory. $H_{\mathrm{eff}}^{(3)}$ allows us to predict the degeneracy point of the three-spin term using the degeneracy point of the two-spin term with the following energies:

$$E_{S=3/2}-E_{|0\rangle_3}=\frac{6t^2}{U}\cos\left(\frac{\pi\Phi_{(2)}}{\Phi_0}\right)+\frac{6\sqrt{3}t^3}{U^2}\sin\left(\frac{2\pi\Phi_{(3)}}{\Phi_0}\right), \tag{22}$$

$$E_{|1\rangle_3}-E_{|0\rangle_3}=\frac{12\sqrt{3}t^3}{U^2}\sin\left(\frac{2\pi\Phi_{(3)}}{\Phi_0}\right). \tag{23}$$

From the dotted line in the top panel of Fig. 8 and Eq. (22) we find $\Phi_0/4A'\approx 2.2T$. Using Eq. (23), we predict the dashed line to cross the x axis near $B\approx 1.5$ T, where we take A to be the area of an equilateral triangle with 40 nm side lengths. A similar analysis yields good agreement for the bottom panel of Fig. 8.

The slope of the energy splitting between the two lowest states in Fig. 8 allows us to estimate t/U for this system using Eq. (22). t/U is largest and only weakly magnetic field dependent at low B. Taking $A+\frac{3}{2}A'$ from above and $v=0$, we obtain $t/U\simeq 0.09$ for the top panel and 0.19 for the bottom panel which shows that our expansion in t/U is consistent. For $N=3$, only odd powers of t_{ij} allow linear magnetic field dependence in the splitting, showing that, excluding double occupancy, the magnetic field dependence captured by the chiral term is accurate up to $\vartheta(t^5/U^4)$.

V. CONCLUSION

We show in this work that the Heisenberg model description of the qubit coupling in the quantum-dot spin-quantum-computer architecture applies only in a limited regime of the parameter space. In the GaAs-quantum-dot exchange-gate architecture, the Heisenberg spin Hamiltonian description applies only in the intermediate regime $R/a\gtrsim 1$ and $\omega_c/\omega_0\lesssim 1$. Using the exact diagonalization technique one can map out the precise low-lying Hilbert space, and consequently use this information in the design of the quantum-computer architecture. We have also discussed an interesting and nontrivial level-crossing periodicity in the singlet-triplet energetics. Precise knowledge of the associated, low-energy Hilbert space could, in principle, be used to protect quantum information encoded in the electron spin.

Generalizing our exact diagonalization technique to spin-cluster qubits formed by a two-dimensional array of electron spins localized in tunnel-coupled quantum dots, we show that the chiral term associated with the quantum phase picked up by an electron enclosing the magnetic flux through closed loops must be included in the spin Hamiltonian. The existence of the chiral term in the looped spin-cluster qubits modifies the Heisenberg interaction and is in some sense a decoherence mechanism for the simple exchange-gate architecture (since the two-qubit SWAP operation is no longer determined by just the Heisenberg exchange Hamiltonian). We show in this paper how precise knowledge of the cluster geometry, combined with exact diagonalization, provides us with the multispin Hamiltonian which would be required for quantum computation with two- or three-dimensional spin-cluster qubits. Strictly one-dimensional spin-cluster qubits, which do not have any topological looping, have a small (but nonzero) chiral contribution and are therefore described, for the most part, by the Heisenberg Hamiltonian in the appropriate subspace of magnetic field, confinement, and dot-geometry parameters.

We emphasize that in this article we have considered a relatively simple model, defined by Eqs. (1) and (2), for determining the applicability of the Heisenberg interaction in describing the exchange-gate operation. Differences in the confinement potential may change some of the quantitative aspects of our results but as long as the confinement consists of smooth potential wells, there should be qualitative agreement. The key issue we have addressed in this work is the regime of validity of the Heisenberg exchange-gate operation in coupled semiconductor quantum-dot quantum-computer architectures as appropriate, for example, in GaAs-based quantum-dot systems. In practice, we have obtained the conditions and constraints necessary for a coupled-qubit system to behave as a coherent molecule as opposed to two decoupled atoms. Adiabatic tuning between these two regimes enables the swap idea underlying the exchange gate. Of course, the issue of He atom-to-molecule transition in coupled-quantum-dot systems as well as our discussion of the exchange oscillations in the coupled-dot system as a function of the applied magnetic field have implications beyond quantum computation. For example, a direct experimental observation of the exchange oscillations is of interest in quantum-dot physics.

Finally we mention that there are many other factors beyond the scope of our work [i.e., beyond the model defined in Eqs. (1) and (2)] which affect the operation of the exchange gate. We cite three such example of recent interest which have been considered in the literature: inhomogeneous magnetic field effects [39], spin-orbit coupling [40,41], and multivalley quantum interference [42].

ACKNOWLEDGMENTS

We would like to thank J. K. Jain and K. Park for many helpful discussions. This work is supported by ARO-ARDA and NSA-LPS.

[1] D. Loss and D. P. DiVincenzo, Phys. Rev. A **57**, 120 (1998).
[2] B. E. Kane, Nature (London) **393**, 133 (1998).
[3] R. Vrijen *et al.*, Phys. Rev. A **62**, 012306 (2000).
[4] X. Hu and S. Das Sarma, Phys. Rev. A **61**, 062301 (2000).
[5] R. de Sousa and S. Das Sarma, Phys. Rev. B **67**, 033301 (2003).
[6] J. M. Elzerman, R. Hanson, L. H. W. van Beveren, B. Wilfkamp, L. M. K. Vandersypen, and L. P. Kouwenhoven, Nature (London) **430**, 431 (2004); D. Rugar, R. Budakian, H. J. Mamin, and B. W. Chui, *ibid.* **430**, 329 (2004); M. Kroutvar, V. Ducommun, D. Heiss, M. Bichler, D. Schuh, G. Abstreiter, and J. J. Finley, *ibid.* **432**, 81 (2004); D. M. Zumbuhl, C. M. Marcus, M. P. Hanson, and A. C. Gossard, Phys. Rev. Lett. **93**, 256801 (2004).
[7] A. Harju, S. Siljamaki, and R. M. Nieminen, Phys. Rev. Lett. **88**, 226804 (2002).
[8] V. W. Scarola and S. Das Sarma, e-print cond-mat/0311463.
[9] G. Burkard, D. Loss, and D. P. DiVincenzo, Phys. Rev. B **59**, 2070 (1999).
[10] A. Mizel and D. A. Lidar, Phys. Rev. Lett. **92**, 077903 (2004); Phys. Rev. B **70**, 115310 (2004).
[11] J. Levy, Phys. Rev. Lett. **89**, 147902 (2002).
[12] F. Meier, J. Levy, and D. Loss, Phys. Rev. Lett. **90**, 047901 (2003); Phys. Rev. B **68**, 134417 (2003).
[13] S. C. Benjamin and S. Bose, Phys. Rev. Lett. **90**, 247901 (2003).
[14] D. P. DiVincenzo, D. Bacon, J. Kempe, G. Burkard, and K. B. Whaley, Nature (London) **408**, 339 (2000).
[15] V. W. Scarola, K. Park, and S. Das Sarma, Phys. Rev. Lett. **93**, 120503 (2004).
[16] J. K. Pachos and E. Rico, e-print quant-ph/0404048.
[17] J. K. Jain and T. Kawamura, Europhys. Lett. **29**, 321 (1995).
[18] A. H. MacDonald, S. M. Girvin, and D. Yoshioka, Phys. Rev. B **37**, 9753 (1988).
[19] M. Takahashi, J. Phys. C **10**, 1289 (1977).
[20] P. G. J. van Dongen, Phys. Rev. B **49**, 7904 (1994).
[21] D. S. Rokhsar, Phys. Rev. Lett. **65**, 1506 (1990).
[22] D. Sen and R. Chitra, Phys. Rev. B **51**, 1922 (1995).
[23] X. G. Wen, F. Wilczek, and A. Zee, Phys. Rev. B **39**, 11413 (1989).
[24] F. D. M. Haldane, Phys. Rev. Lett. **51**, 605 (1983).
[25] J. K. Jain, Phys. Rev. Lett. **63**, 199 (1989).
[26] H. Yi and H. A. Fertig, Phys. Rev. B **58**, 4019 (1998).
[27] V. W. Scarola and J. K. Jain, Phys. Rev. B **64**, 085313 (2001).
[28] X. Hu and S. Das Sarma, Phys. Rev. A **66**, 012312 (2002).
[29] E. Knill, R. Laflamme, and L. Viola, Phys. Rev. Lett. **84**, 2525 (2000).
[30] L. Viola, E. Knill, and S. Lloyd, Phys. Rev. Lett. **85**, 3520 (2000).
[31] K. Nakamura, Y. Nakahara, and A. R. Bishop, Phys. Rev. Lett. **54**, 861 (1985).
[32] J. Kempe, D. Bacon, D. A. Lidar, and K. B. Whaley, Phys. Rev. A **63**, 042307 (2001).
[33] D. A. Lidar, I. L. Chuang, and K. B. Whaley, Phys. Rev. Lett. **81**, 2594 (1998).
[34] D. Bacon, J. Kempe, D. A. Lidar, and K. B. Whaley, Phys. Rev. Lett. **85**, 1758 (2000).
[35] V. Fock, Z. Phys. **47**, 446 (1928); C. G. Darwin, Proc. Cambridge Philos. Soc. **27**, 86 (1930).
[36] M. Wagner, U. Merkt, and A. V. Chaplik, Phys. Rev. B **45**, R1951 (1992).
[37] M. V. Berry, Proc. R. Soc. London, Ser. A **392**, 45 (1984).
[38] G. S. Jeon, K. L. Graham, and J. K. Jain, Phys. Rev. Lett. **91**, 036801 (2004).
[39] X. Hu, R. de Sousa, and S. Das Sarma, Phys. Rev. Lett. **86**, 918 (2001); R. de Sousa, X. Hu, and S. Das Sarma, Phys. Rev. A **64**, 042307 (2001).
[40] K. V. Kavokin, Phys. Rev. B **64**, 075305 (2001).
[41] N. E. Bonesteel, D. Stepanenko, and D. P. DiVincenzo, Phys. Rev. Lett. **87**, 207901 (2001).
[42] B. Koiller, X. Hu, and S. Das Sarma, Phys. Rev. Lett. **88**, 027903 (2002); Phys. Rev. B **66**, 115201 (2002); B. Koiller, R. B. Capaz, X. Hu, and S. Das Sarma, *ibid.* **70**, 115207 (2004).